Chemie Ingenieur Technik

Aseptic zero discharge fluid dynamic gauging for measuring the thickness of soft layers on surfaces

Journal:	*Chemie Ingenieur Technik*
Manuscript ID	Draft
Wiley - Manuscript type:	Kurzmitteilung
Date Submitted by the Author:	n/a
Complete List of Authors:	Wang, Shiyao; University of Cambridge, Department of Chemical Engineering and Biotechnology Schlüter, Florian; Technical University of Braunschweig, Institute for Chemical and Thermal Process Engineering Gottschalk, Nathalie; Technical University of Braunschweig, Institute for Chemical and Thermal Process Engineering Scholl, Stephan; Technical University of Braunschweig, Institute for Chemical and Thermal Process Engineering Wilson, D.; University of Cambridge, Department of Chemical Engineering and Biotechnology Augustin, Wolfgang; Technical University of Braunschweig, Institute for Chemical and Thermal Process Engineering
Keywords:	Biofouling, Dickenmessung, Rauigkeit, Analytik, Steriltechnik

Aseptic zero discharge fluid dynamic gauging for measuring the thickness of soft layers on surfaces

Aseptisches Fluid Dynamic Gauging zur Messung der Dicke von weichen Schichten auf Oberflächen

Shiyao Wang[1], Florian Schlüter[2], Nathalie Gottschalk[2], Stephan Scholl[2], D. Ian Wilson[1] and Wolfgang Augustin[2,*]

[1]Department of Chemical Engineering and Biotechnology, New Museums Site, Pembroke Street, Cambridge, CB2 3RA, UK

[2]Technische Universität Braunschweig, Institute for Chemical and Thermal Process Engineering, Langer Kamp 7, Braunschweig, Germany

*Corresponding author: w.augustin@tu-braunschweig.de

Abstract

A bench-top device that can be used to perform fluid dynamic gauging measurements of soft solid layers with zero net liquid discharge and potentially under aseptic (closed system) conditions is demonstrated. Testing results are presented for Newtonian liquids with a range of viscosities: deionised water, 8 wt% and 10 wt% sucrose solutions, 18 wt% glycerol/water solutions and a paraffin oil (1.12 - 1000 mPa s). The experimental data for discharge coefficient, C_d, against clearance/nozzle throat diameter, h/d_t, gave good agreement with CFD simulations and the correlation presented by Tuladhar et al. [1]. The influence of surface roughness was studied by making measurements on a series of commercial sandpapers. The rough surfaces gave rise to systematic differences in C_d from those obtained with smooth substrates which could not be corrected for using the height of the asperity peaks and careful calibration is therefore required when gauging rough surfaces.

Ein Laboranalysemethode zur Messung der Schichtdicke von weichen Feststoffablagerungen mit Hilfe des Fluid Dynamic Gauging wird vorgestellt. Dabei wird im Gegensatz zu bisherigen Anwendungen kein Fluid aus dem System entnommen, was einen aseptischen Betrieb ermöglicht. Erste Ergebnisse werden gezeigt für Newtonische Flüssigkeiten in einem weiten Viskositätsbereich: entionisiertes Wasser, 8 Gew.-% and 10 Gew.-% Zuckerlösung, 18 Gew.-% Glyzerin/Wasser-Lösung und ein Paraffinöl (1,12 - 1000 mPa s). Die experimentellen Daten für die Abhängigkeit des dimensionslosen Massenstrom C_d vom Verhältnis Abstand/Düsendurchmesser h/d_t, zeigen eine gute Übereinstimmung mit CFD-Simulationen und der von Tuladhar et al. [1] präsentierten Korrelation.

Der Einfluss der Oberflächenrauhigkeit wurde mit Hilfe verschiedene Sandpapiere untersucht. Es ergaben sich systematische Abweichungen von den Ergebnissen mit glatten Oberflächen, was nicht durch eine einfache Berücksichtigung der Rauheitsspitzen korrigiert werden konnte. Hier ist eine umfangreichere Kalibration erforderlich.

Key words: fluid dynamic gauging, aseptic, scanning, film thickness, surface roughness

1 Introduction

Biofilms, tissue cultures and proteinaceous fouling deposits are all examples of soft solid layers on surfaces. They are soft because they contain large amounts of liquid (*i.e.* high voidage) and the structural material has high elasticity or low strength. When removed from their natural (immersed) environment they often collapse. This creates problems when measuring the thickness of such layers, as non-contact techniques such as tomography are often expensive and require detailed calibration. Optical methods such as laser scanning confocal microscopy require the material or the liquid to be transparent to the light used.

The technique of fluid dynamic gauging (FDG) was developed by Tuladhar *et al*. [1] to allow the thickness of such layers to be measured *in situ*, in real time and relatively cheaply. Liquid is withdrawn or ejected, slowly, from a convergent nozzle located near the surface of the layer. The pressure drop and mass flow rate through the nozzle are measured, and together give an indication of how close the nozzle is to the layer surface. The nozzle location relative to the substrate is measured separately and the difference between the two distances gives the thickness of the layer. FDG does not require knowledge of physical and chemical properties of the solution and the layer (they can be opaque) except of the presence of a locally stiff surface. The forces exerted by the FDG flow can be estimated with confidence from computational fluid dynamics simulations (Chew *et al*. [2, 3]; Wang and Wilson [4]). The technique has been used to study the growth (fouling) and removal (cleaning) of a range of layer materials, and a scanning version of the device allowed different regions of a layer or substrate to be investigated (Gordon *et al*. [5]). A comprehensive description of the application spectrum is given in Augustin *et al.* [6].

In the early versions, the pressure drop across the nozzle was fixed and the flow rate measured. This required the use of significant volumes of liquid in an unsealed configuration. Given that many soft solid layers of interest would ideally be studied in a contained environment, *e.g*. for microbiological containment, and/or the inventory of liquid kept small, the technique of zero net discharge FDG (ZFDG) was developed. In this mode, the flow rate is set by a syringe pump and the pressure drop

across the nozzle measured. The liquid is ejected and withdrawn from the test chamber in successive phases, so that no liquid enters or leaves the system. The operating principles of ZFDG were demonstrated by Yang *et al*. [7] and a system for studying layers on flat substrates was presented by Wang and Wilson [4]. Lemos *et al*. [8] bespoke ZFDG device to measure the thickness of *Pseudomonas fluorescens* biofilms on cylinders with a ZFDG unit.

The above ZFDG systems did not offer completely aseptic operation (small air channels were required to allow pressure equalisation). This paper describes the development of an aseptic ZFDG device which requires a modest volume of liquid (approximately two litres): the ability to use different liquids is demonstrated by calibration testing with liquids with a range of viscosities. The device features scanning capability and this is demonstrated in a short study of the effect of surface roughness on measurement. The latter studies also allowed the influence of surface roughness to be quantified, as layers of soft solids are sometimes uneven.

2 ZFDG Apparatus

ZFDG measurements are based around a convergent nozzle with throat diameter d_t, through which liquid is withdrawn or ejected at a controlled rate by means of a syringe pump. The nozzle geometry and dimensions for this device are shown in Figure 1: its hydrodynamics in ejection and suction mode were studied experimentally and the results compared with computational fluid dynamics (CFD) simulations by Wang and Wilson [4].

The aseptic ZFDG test rig is similar to that used by Wang and Wilson [4] but features a smaller, (cylindrical) liquid reservoir, an *x-y* stage which allows the substrate and layer being tested to be translated for scanning, and a method for isolating the contents from the surroundings. Figure 2 is a schematic of the apparatus while Figure 3 shows photographs of the system and key components. The reservoir (height 150 mm, diameter 130 mm, operating volume in these tests = 2 L) was constructed from Perspex™ so that the layer could be monitored visually during testing.

Isolation is achieved by means of an aluminium foil (or flexible polypropylene film) which is secured to the top edge of the reservoir and to a ring on the nozzle mounting. The nozzle passes through a septum on the ring, providing a gas-tight seal. The airspace within the tent can be exchanged or purged as necessary. The flexibility of the film allows it to change shape as the liquid level changes when the gauging fluid is withdrawn or added to the reservoir via the nozzle, and adjusts with any transverse motion.

Liquid is fed or withdrawn by a computer controlled syringe pump (Hamilton® Glass, d_i =32.6 mm syringe; Harvard Apparatus PHD Ultra™ Series pump). The accuracy of the flow rate, $\dot{m}$, was

measured as 1% of the set value. The nozzle (dimensions in Figure 1) was constructed from 304 stainless steel and is installed at the end of a long (310 mm) stainless steel tube. The nozzle is detachable so that different throat diameters and nozzle shapes can be employed as required. The nozzle vertical position is controlled by a stepper motor (Zaber Technologies, T-LSR075B, CE). Displacement in the horizontal plane in these tests was achieved by moving the reservoir and test stage using a manual *x*-*y* stage (travel 95 mm ×75 mm, ± 0.01 mm; KAMI, Germany): an automated stage would allow scanning as reported by Gordon *et al*. [5]. The nozzle vertical position (distance to the uncoated surface, labelled h_0 on Figure 1) is determined using feeler gauges with known thickness (*e.g.* 0.1 mm). Calibration tests are usually started with h_0 = 1.0 mm.

The pressure drop across the nozzle, ΔP, was measured by a pressure transducer (SensorTechnics HMAP001BU7H5) with an operating limit of approximately 7 kPa. Data collection and processing was performed with a LabVIEW® (National Instruments™) application, which also controlled the nozzle location and syringe pump motion. The LabVIEW code included a pressure difference cut-out to avoid damage to the pressure transducer.

3 Material and Methods

3.1 Calibration

The flow rate-pressure drop relationship is quantified in terms of the discharge coefficient, C_d, which is the ratio of the actual to the ideal flow rates, *viz*.

$$C_d = \frac{\dot{m}_{actual}}{\dot{m}_{ideal}} = \frac{4\dot{m}}{\pi d_t^2 \sqrt{2\rho\Delta P}} \quad (1)$$

where ρ is the liquid density. The hydrodynamics of the flow through the nozzle are quantified in terms of the throat Reynolds number, defined

$$Re_t = 4\dot{m}/\pi\mu d_t \quad (2)$$

where μ is the liquid viscosity. For a given value of Re_t, C_d is very sensitive to the clearance between the nozzle and the surface, labelled h (with layer present) or h_0, for $h_0/d_t < 0.3$. In dimensionless terms,

$$C_d = f\left(\frac{h_0}{d_t}, Re_t\right) \quad (3)$$

For a given flow rate (and thus Re_t), measurement of ΔP allows C_d to be evaluated and the distance of the nozzle from the test surface (uncoated substrate or layer) calculated. Tuladhar *et al*. [1] fixed ΔP and measured $\dot{m}$: in ZFDG testing the reverse is done.

Calibration tests were performed using clean, flat stainless steel substrates (50 mm diameter, 3 mm thick). The nozzle, initially distant from the substrate, was moved towards the surface in steps of 0.1 mm, 0.05 mm and 0.02 mm as h_0 decreased. Liquid was alternately ejected then withdrawn at each nozzle location. The control software waited for the ΔP reading to reach steady state, which took about 4 s. The pressure drop for the static (no flow) steady state was also measured so that any hydrostatic component arising from the difference in liquid levels could be accounted for. A feedback loop acted to stop and then withdraw the nozzle when the pressure drop approached the sensor's limit. In the tests presented here the nozzle-surface clearance reached approximately 0.1 mm, subject to the above pressure drop criterion. Calibration plots (C_d *vs* h_0/d_t) were then generated. Calibration tests obtained with the nozzle moving away from the substrate gave identical results.

Measured values of C_d are compared with values obtained from CFD simulations and a correlation based on experimental values, obtained for a similar nozzle with fixed ΔP and $\dot{m}$ measured, by Tuladhar *et al*. [1]. The simulations were performed using the COMSOL Multiphysics modelling platform. A detailed account of the computational methods and solution techniques is given in Wang and Wilson [4].

3.2 Test liquids

Calibration tests were performed with a range of Newtonian liquids: deionised water, paraffin oil, and solutions of glycerol and sucrose in deionised water. The physical properties of the gauging liquids are presented in Table 1. Tests were performed at 16.5 ºC and atmospheric pressure. Flow rates of 5–50 ml/min were used, giving Re_t values ranging from 0.36 - 943. Only one flow rate, of 20 ml/min, was used with 18 wt% glycerol and paraffin oil, the high viscosity of the latter giving $Re_t = 0.36$.

3.3 Test surfaces

The stainless steel disc was relatively smooth. Its arithmetic mean height of roughness, R_a (see Figure 4(*c*)) of 0.2 μm was considerably smaller than the smallest clearance used in ZFDG measurements (approximately 100 μm). The effect of surface roughness was investigated by gluing strips of sand paper (3M) of different grit sizes to a plate (see Figure 4 (*a*)) and generating calibration plots for each surface type in a series of tests. The roughness data reported by Mell [9] for similar materials are listed in Table 2. Deionised water was used as the gauging liquid and the nozzle was moved across the disc to make a series of measurements as shown in Figure 4(*a*).

On the smooth surface the nozzle location was zeroed by using feeler gauges of known thickness. The thickness of sandpaper, δ_s, was measured by a digital micrometer (Mitutoyo, Japan) with a stub diameter of 10 mm, giving thickness ranging from 0.27 mm (P240) to 0.50 mm (P120). The initial estimate of the clearance, h, when performing calibration tests with sandpaper was calculated using

$$h = h_0 - \delta_s \quad [4]$$

Measuring ΔP for set values of $\dot{m}$ gave calibration plots of C_d *vs* h/d_t. The h values were corrected to the true value of the nozzle – surface (rough) clearance, h_{true}, by (Figure 4(c))

$$h_{true} = h + R_p \quad [5]$$

where R_p is the average height between the peak and mean planes (see Table 2). Calibration plots show sets of C_d *vs* h_{true}/d_t.

4 Results and Discussion

4.1 Reproducibility

Reproducibility tests were performed using deionised water at a flow rate of 20 ml/min and 16.5 ºC (Re_t = 377). The clean steel surface was gauged at a single point 10 times for each value of h_0 (from 0.5 mm to 0.1 mm, with decrements of 0.1 mm). The C_d values in Figure 5 show very good reproducibility, with standard error in both ejection and suction modes of less than 0.2 %. The region for ZFDG measurements, where C_d is usefully sensitive to h_0/d_t, can be seen to lie between $0.05 < h_0/d_t < 0.25$, in agreement with Yang *et al*. [7] and Wang and Wilson [4]. At higher values of h_0/d_t, C_d reaches an asymptote (in this case ~ 0.8, depending on the imposed flowrate). The agreement with CFD predictions is good.

The main uncertainties in measurements arose from the accuracy of zeroing the nozzle–substrate clearance, estimated at ± 5 μm, since ΔP was very sensitive to lower values of h. This was minimised by using different feeler gauges to crosscheck the initial clearance. The accuracy of the mass flow measurements was good (around 1 %). The pressure transducer uncertainty was reduced by increasing the signal to noise ratio using Fast Fourier Transform (FFT) analysis.

4.2 Different gauging liquids

Figure 6 shows calibration plots for the different liquids in Table 1 for (*a*) ejection and (*b*) suction, respectively, at a flowrate of 20 ml/min. Suction mode gives lower C_d values than ejection, which is due to a higher pressure drop through the nozzle at these Reynolds numbers associated with the presence of a recirculation zone downstream of the nozzle throat (see Chew *et al*. [2]). The error bar for each datum is dominated by the uncertainty in the pressure measurement and these are smallest at low clearance: there is thus higher reliability in the pseudo linear region (see insets). Also shown on the plot are the results from CFD simulations for deionised water in both ejection and suction modes. The predictions again give good agreement, within experimental uncertainty.

The results for solutions with low viscosity, namely water and the sucrose solutions, exhibit a common trend of a pseudo-linear region ($0.1 < h_0/d_t < 0.24$) followed by an approach to an asymptote

at large h_0/d_t. With the more viscous liquids, namely 18 % glycerol solution and the paraffin, the contribution from viscous dissipation dominates that from inertia: smaller C_d values are obtained and the transition is more gradual. The ideal flow term in the definition of C_d, Equation (1), is based on an inertial result, so C_d is not expected to describe the pressure drop at low Re_t well. This was discussed at length by Chew *et al*. [3]. For ZFDG testing, the overall ΔP increases slowly as the nozzle approaches the substrate and the usefully linear region is hard to achieve with viscous gauging liquids. This result, combined with the potential for disruption of the layer caused by the high shear stress imposed by the flow on the surface, means that highly viscous liquids are less well suited for ZFDG applications.

4.3 Effect of gauging flow rate

The effect of gauging flow rate (and Re_t) on C_d was investigated for the less viscous liquids. The influence of flow rate has been studied previously for 'mass flow' FDG, where the pressure drop (hydrostatic head) is controlled and the flow rate measured, by Tuladhar *et al*. [1] and Chew *et al*. [2, 3]). The objective of this work was to establish whether similar effects are seen in 'pressure mode' measurements, where the flow rate is controlled. The results in Figure 7 show similar trends to those noted above: C_d was generally larger for ejection than suction; C_d increases with h_0/d_t, and, in the usefully linear region, increases weakly with Re_t. In the asymptotic region (Figure 7(a)), C_d is approximately 0.8 for all Re_t. These observations are consistent with the findings of Chew *et al*. [2]. Figure 7(b-d) shows that for smaller h_0/d_t values, the effect of viscosity is not accounted for by Re_t, as postulated in Equation (3). This is consistent with the influence of viscous dissipation and the use of an inertial loss term in defining C_d, as noted above. The data obtained for smaller flowrates, such as 5 ml/min, are less consistent but agree within the experimental uncertainty which arises from the sensitivity of the pressure measurements.

The agreement with 'mass flow' FDG was investigated further by comparing the results obtained in suction mode with the correlation for C_d obtained by Tuladhar *et al*. [1] from experimental data collected over the range $400 < Re_t < 2000$ for a nozzle similar to that in Figure 1. Its dimensions were: $d_t = 1.0$ mm, $d_i = 4.0$ mm, $w_r = 0.5$ mm and $w_e = 0.1$ mm. They reported

$$1000C_d = \left(0.3571 \exp\left[-5.0613\sqrt{\frac{h_0}{d_t}}\right]\right) Re_t + \left(-70.3 + 3721.2\left(\frac{h_0}{d_t}\right) - 2238.3\left(\frac{h_0}{d_t}\right)^2\right) \quad (6)$$

The results from the present work, for $h_0/d_t = 0.1$ and 0.14, are plotted alongside Tuladhar *et al*.'s data in Figure 8: there are excellent agreements for the water values. There is also good agreement with the CFD simulation results for deionized water over the range $90 < Re_t < 1200$. For a given value of h_0/d_t Equation (6) predicts a linear relationship, *viz.*

$$h_0/d_t = 0.14 \qquad C_d = 5.37 \times 10^{-5} Re_t + 0.41 \quad (7)$$

$h_0/d_t = 0.10$ $\quad C_d = 7.20 \times 10^{-5} Re_t + 0.28$ (8)

The Figure shows reasonably good agreement with the water data for $Re_t > 300$. There is poorer agreement for lower Re_t and for the viscous liquids.

The CFD simulations have been performed for the current nozzle geometry, *i.e.* d_t = 1.0 mm, d_i = 5.9 mm, w_e = 0.15 mm, w_r = 1.0 mm and θ = 45°. By applying the simulation protocol proposed by Wang and Wilson [4], C_d for both ejection and suction modes were extracted and the empirical correlation (Equation (3)) was investigated. C_d is a relatively weak function of ln(Re_t) within the useful measurement region, $0.1 < h_0/d_t < 0.24$, *viz.*

$$C_{d,E} = \left(0.036 + 1.093\left(\frac{h_0}{d_t}\right) - 5.571\left(\frac{h_0}{d_t}\right)^2\right)\ln(Re_t) + \left(-0.689 + 5.094\left(\frac{h_0}{d_t}\right) + 0.576\left(\frac{h_0}{d_t}\right)^2\right) \quad (9)$$

$$C_{d,S} = \left(0.068 - 0.134\left(\frac{h_0}{d_t}\right) + 0.105\left(\frac{h_0}{d_t}\right)^2\right)\ln(Re_t) + \left(-0.54 + 6.49\left(\frac{h_0}{d_t}\right) - 13.509\left(\frac{h_0}{d_t}\right)^2\right) \quad (10)$$

This model effectively corrects Tuladhar's [1] model for the lower range of Re_t, especially from 90 to 400 and agrees with larger Re_t above 400 in the laminar flow regime.

There is thus good agreement between the two modes of FDG measurement. ZFDG offers robust and reliable operation while offering the capacity to use small liquid inventory and potentially hazardous substances.

4.4 Effect of surface roughness

The smooth and sandpaper surfaces were studied using deionised water at 16.5 ºC as the gauging liquid with flow rates ranging from 10 – 40 ml/min, corresponding to Re_t = 189 – 754. Surface roughness had no effect at large clearance values. Examples of results are presented for $h/d_t = 0.10$ (of interest for gauging measurements) for both ejection and suction modes in Figure 9.

For both smooth and rough surfaces, C_d increases as flowrate and clearance increases, which agrees with Equation (6). For a given combination of Re_t and h/d_t, C_d is larger for a rougher surface. This is due to the systematic effect of roughness elements on the estimated clearance, presented in Figure 4(c). For rougher surfaces, such as P120, the peak to trough region is available for liquid flow so the true thickness of the flow region is larger than the set value (equation (5)): h_0/d_t is therefore larger than h/d_t, and C_d is consequently greater.

The values for P150 and P180 lie within the measurement uncertainty. The difference in roughness of two surfaces is ~ 0.5 μm, which is lower than the resolution (~ 5 μm) of the gauging technique.

Figure 9 indicates that roughness elements of the size and nature found on sandpapers introduce significant uncertainty in the ZFDG measurements. One method for correcting for the known

roughness based on peak heights is shown in Figure 4(c), yielding Equation (5). Figure 10 shows series of corrected data sets presented as plots of C_d *vs* h_{true}/d_t. Data for two flowrates are presented: seven flow rates were tested. The correction protocol gives good agreement for ejection at higher flowrates, *i.e.* $500 < Re_t < 754$, but for lower ejection flow rates and in all suction mode tests C_d is systematically underestimated. The correction protocol gives good agreement between the rough surfaces, but differs from the smooth values by up to 0.1. This difference is significant for measurements of absolute layer thickness. The good agreement between corrected values indicates that the correction protocol needs refinement. The peak height calculation gives an approximate account for the difference in flow area: the increase in surface area of the substrate, which will increase ΔP and reduce C_d, has not been included. In the absence of a more reliable correction protocol, careful calibration using surfaces of similar roughness would be needed in order to make measurements of such layers.

5 Conclusions

The technique of fluid dynamic gauging was extended for the use with zero net liquid discharge and potentially under aseptic conditions. A new measuring device was designed and manufactured. Proof-of-concept results have been obtained for a series of Newtonian liquids, ranging in viscosity from water to paraffin oil. The discharge coefficient is usefully sensitive to the nozzle-substrate clearance in the range $0.05 < h_0/d_t < 0.25$ for all but the most viscous liquid, for which the sensitivity is poorer. These results showed good agreement with computational fluid dynamics simulations and, within the range of testing, the correlation presented by Tuladhar *et al*. [1].

Testing on surfaces with mixed roughness profiles demonstrated that the device can be used in scanning mode. Data obtained with a series of commercial sandpapers indicated that surface roughness can have a significant effect on ZFDG measurements, which could not be accounted for by a simple peak-to-height correction. Careful calibration is therefore required when making measurements on such surfaces.

Acknowledgements

Development of the ZFDG concept was supported by the Royal Society's Paul Instrument Fund. The test rig was constructed by the technical team, in particular Karl Karrenführer, Jörg Leppelt and Sven Lorenzen, at the Institute for Chemical and Thermal Process Engineering, Technische Universität Braunschweig. Funding from Fitzwilliam College for Shiyao Wang is also gratefully acknowledged.

6 Symbols used

Roman

C_d	[-]	Fluid discharge coefficient
d_i	[m]	Inner diameter
d_t	[m]	Diameter of nozzle throat
h_{true}	[m]	True initial gauging clearance
h_0	[m]	Nozzle-substrate clearance
i.d.	[m]	Internal diameter
$\dot{m}$	[kg·s^{-1}]	Mass flow rate
ΔP	[kg·m^{-1}·s^{-2}]	Differential pressure ($\Delta P_{dyn} - \Delta P_{static}$)
ΔP_{dyn}	[kg·m^{-1}·s^{-2}]	Dynamic pressure measurement
ΔP_{static}	[kg·m^{-1}·s^{-2}]	Static pressure measurement
R_a	[m]	Arithmetical mean height
Re_t	[-]	Reynolds number at nozzle throat
R_p	[m]	Average height between highest peak and mean plane
R_z	[m]	Average height between highest peak and deepest valley
w_e	[m]	Nozzle rim width
w_r	[m]	Nozzle rim thickness

Greek

δ_{true}	[m]	True thickness of sandpaper
δ_s	[m]	Thickness of sand paper measured by Micrometer
Φ	[m]	Diameter
ε	[-]	Uncertainty
μ	[kg·m^{-1}·s^{-1}]	Fluid viscosity
ρ	[kg·m^{-3}]	Fluid density

Acronym

CFD	Computational fluid dynamics
DAQ	Data acquisition
FFT	Fast Fourier Transform
LabVIEW	Laboratory virtual instrument engineering workbench
PT	Pressure transducer
SS	Stainless Steel
ZFDG	Zero (net) discharging fluid dynamic gauging

7 References

[1] T.R. Tuladhar, W.R. Paterson, N. Macleod, and D.I. Wilson. *The Can. J. Chem. Eng.* **2000**, 78(October). DOI:10.1002/cjce.5450780511

[2] J.Y.M. Chew, S.S.S. Cardoso, W.R. Paterson, and D.I. Wilson, *Chem. Eng. J.* **2004a**, 59(16). DOI:10.1016/j.ces.2004.03.042

[3] J.Y.M. Chew, W.R. Paterson, and D.I. Wilson, *J. Food Eng.* **2004b**, 65(2). DOI:10.1016/j.jfoodeng.2004.01.013

[4] S. Wang & D.I. Wilson, *Ind. Eng. Chem. Res.* **2015**, 54. DOI: 10.1021/acs.iecr.5b01956

[5] P.W. Gordon, A.D.M. Brooker, J.Y.M. Chew, D.I. Wilson, and D.W. York, *Measurement Sci. Tech.* **2010**, 21(8). DOI: 10.1088/0957-0233/21/8/085103

[6] W. Augustin, Y.M.J. Chew, P.W. Gordon, V.Y. Lister, M. Mayer, W.R. Paterson, J.M. Peralta, S. Scholl, and D.I. Wilson, *Chem. Ing. Tech.* **2012**, 84(1). DOI: 10.1002/cite.201100165

[7] Q. Yang, A. Ali, L. Shi and D.I. Wilson, *J. Food Eng.* **2014**, 127. DOI: 10.1016/j.jfoodeng.2013.11.024

[8] M. Lemos, S. Wang, A. Ali, M. Simões, and D.I. Wilson, *Biochem. Eng. J.* **2016**, 106. DOI: 10.1016/j.bej.2015.11.006

[9] B. Mell, **2010**. Sandpaper Roughness Measurement using 3D Profilometry. NANOVEA®

Tables

Table 1. Physical properties of gauging liquids (16.5 ºC)

Gauging liquid	ρ	μ	Re_t (20 ml/min)	Supplier	Symbol
	kg/m^3	mPa.s	-		Figure 8
Deionised water	997.3	1.12	377	N/A	■/ □
8 wt% sucrose	1029.9	1.25	349	Sigma	▲
10 wt% surcrose	1038.1	1.33	331	Sigma	●
18 wt% glycerol	1047.6	1.65	250	Aldrich	N/A
Paraffin oil	860	1000	0.36	Sigma-Aldrich	N/A

Table 2. Sandpaper surface roughness measures, see Figure 4(b): R_a (arithmetical mean height), R_z (average height between highest peak and deepest valley), R_p (average height between highest peak and mean plane), and average particle sizes

Surface	R_a	R_z	R_p	Average particle diameter	Symbol
	µm	µm	mm	µm	Figure 10
Smooth	0.2	0.97	0.0007	N/A	Lines
P240*	~14.26	~169.6	0.12	68	◇
P180	17.43	198.1	0.14	82	△
P150	16.89	229.9	0.17	92 - 100	□
P120	24.41	273.2	0.20	115 - 125	○

* the data are for P220 due to lack of data on P240

Figure legends

Figure 1. Schematic of ZFDG nozzle geometry. h_0 is the clearance between the nozzle and the substrate. Dimensions: θ = 45°, d_t = 1.0 mm, d_i = 5.9 mm, w_e = 0.15 mm, w_r = 1.0 mm. Dotted streamline indicates the flow path taken by the liquid in the ejection phase; the dashed streamline shows that in suction (with flow recirculation which occurs under certain operating conditions)

Figure 2. Schematic of aseptic ZFDG system

Figure 3. Photographs of ZFDG (a) test rig, and (b) detailed view of 1 mm i.d. nozzle and substrate. Labels: A, linear slide; B, pressure transducer; C, gauging tank; D, *x*-*y* table

Figure 4. (*a*) Photograph, plan view of stainless steel disc with strips of sandpaper of different grit sizes attached. The gauging nozzle was moved across trajectory AA. Points indicate where gauging measurements were made; (*b*) Side view (not to scale) schematic of sandpaper thicknesses for zeroing, $\delta_{1\text{-}4}$ – thicknesses of sandpaper (P180, P150, P240 and P120, respectively); (c) Schematic (not to scale) of rough surface: R_p is the average height between highest peak and mean plane, R_a is the mean roughness, δ_s is the thickness measured by micrometer, δ_{true} the true thickness, h_{true} the corrected/true clearance from the nozzle to mean plane of sandpaper. The smooth substrate is the reference plane

Figure 5. Reproducibility of ZFDG measurements on clean steel substrate. Deionised water at 16.5 °C, flow rate 20 ml/min. Ten data sets were collected at each h_0/d_t value from 0.1 to 0.5. The mean C_d value is plotted against h_0/d_t: the standard deviation is less than 0.2 % of each datum (not shown), and uncertainty in h is shown by horizontal error bars. Symbols: open – ejection, solid – suction; dashed line – CFD simulation of ejection test, solid line – simulation of suction tests

Figure 6. Calibration plots (C_d vs h_0/d_t) for the liquids in Table 1 at a flow rate of 20 ml/min, 16.5 °C. (a) ejection; (b) suction. Symbols: triangle – 18 wt% glycerol, Re_t = 250; diamond – paraffin oil, Re_t = 0.36; square – deionised water, Re_t = 377; circle – 8 wt% sucrose solution, Re_t = 349; cross – 10 wt% sucrose solution, Re_t = 331. Dashed line – CFD simulation, ejection: solid line – CFD simulation, suction (both for deionised water). Inserts show C_d *vs* h_0/d_t in the usefully linear region

Figure 7. Effect of throat Reynolds number on C_d for deionised water (squares), 8 % sucrose solution (triangles) and 10 % sucrose solution (circles) in (*i*) ejection (open symbols) and (*ii*) suction (solid symbols) at (*a*) h_0/d_t = 1.0, (*b*) h_0/d_t = 0.14, (*c*) h_0/d_t = 0.12 and (*d*) h_0/d_t = 0.10

Figure 8. Comparison of experimental measurements, CFD simulations and Equations [6] and [10] for (*a*) h_0/d_t = 0.14 and (b) 0.10. Symbols, data: solid – this work, open – Tuladhar *et al*. [1]. Dashed line, Equation [6], solid lines, Equation [10], dotted lines – CFD simulation (deionized water). Gauging liquid: squares - deionised water, triangles - 8 % sucrose solution, circles - 10 % sucrose solution

Figure 9. Effect of surface roughness, expressed as R_a, at Re_t = 189 (square), 283 (circle), 377 (diamond), 472 (triangle), 566 (cross), 660 (asterisk) and 754 (dash) at initial nozzle-substrate clearance (not corrected for roughness) h/d_t = 0.10. (*a*) ejection - black and (*b*) suction - red. The surfaces are (from left to right) smooth, P240, P150, P180 and P120 (note the roughness of P150 is lower than P180 due to the poor quality control (Mell [9]). Representative uncertainty bars shown for one dataset

Figure 10. Calibration curves (C_d vs h_{true}/d_t) on smooth and rough surfaces (the latter have been corrected for measured roughness). Symbols (Table 2): diamond – P240, triangle – P180, square – P150 and circle – P120. Gauging conditions: deionised water (16.5 °C), (*a*) Re_t =

377 and (*b*) Re_t = 754; (*i*) ejection, (*ii*) Suction. Loci are interpolations of experimental data for smooth surfaces

Text for table of contents

A bench-top device that can be used to perform fluid dynamic gauging measurements of soft solid layers with zero net liquid discharge and potentially under aseptic conditions is demonstrated. Testing results are presented for Newtonian liquids with a range of viscosities: deionised water, sucrose solutions, glycerol/water solutions and a paraffin oil. The experimental data for discharge coefficient against clearance/nozzle throat diameter gave good agreement with CFD simulations. The influence of surface roughness was studied by making measurements on a series of commercial sandpapers.

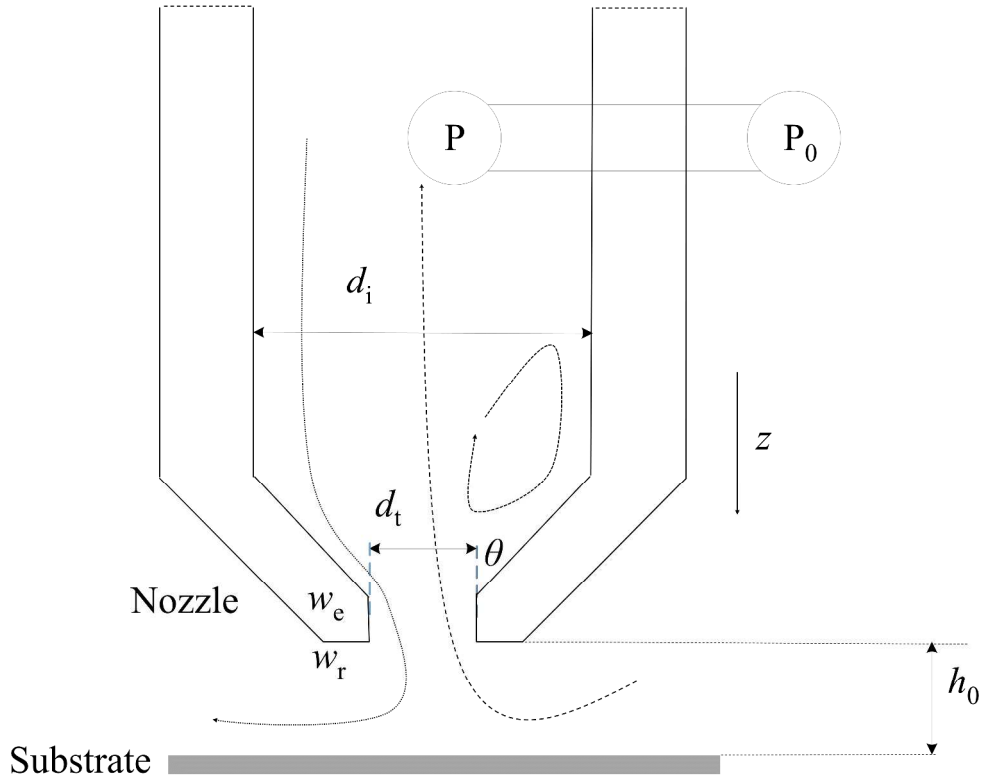

Schematic of ZFDG nozzle geometry. h0 is the clearance between the nozzle and the substrate. Dimensions: θ = 45°, dt = 1.0 mm, di = 5.9 mm, we = 0.15 mm, wr = 1.0 mm. Dotted streamline indicates the flow path taken by the liquid in the ejection phase; the dashed streamline shows that in suction (with flow recirculation which occurs under certain operating conditions)
1921x1515mm (72 x 72 DPI)

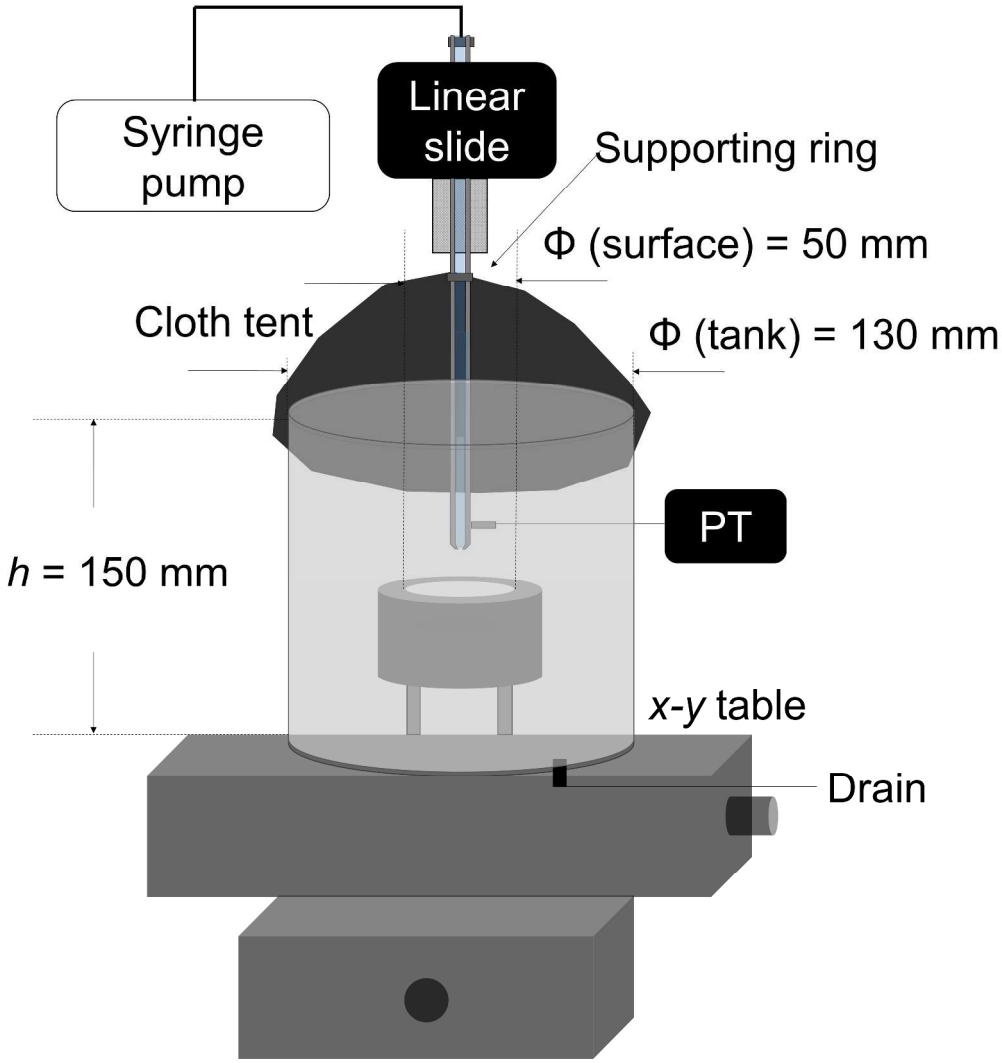

Schematic of aseptic ZFDG system
1405x1509mm (72 x 72 DPI)

(a) (b)

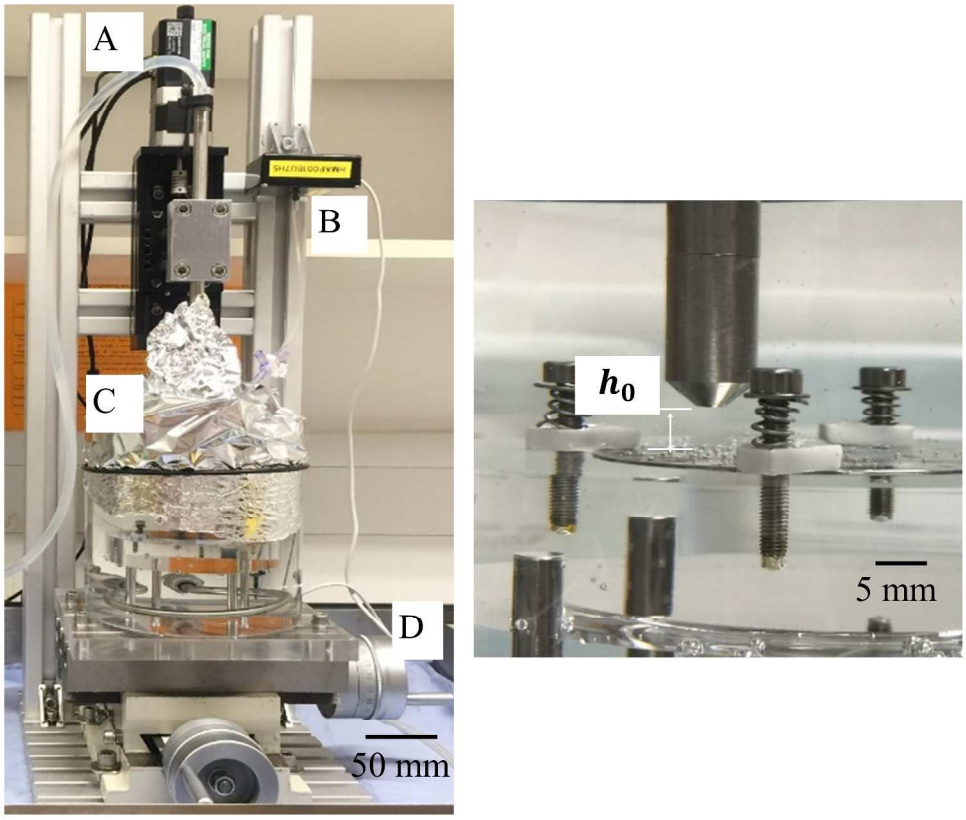

Photographs of ZFDG (a) test rig, and (b) detailed view of 1 mm i.d. nozzle and substrate. Labels: A, linear slide; B, pressure transducer; C, gauging tank; D, x-y table
1651x1507mm (72 x 72 DPI)

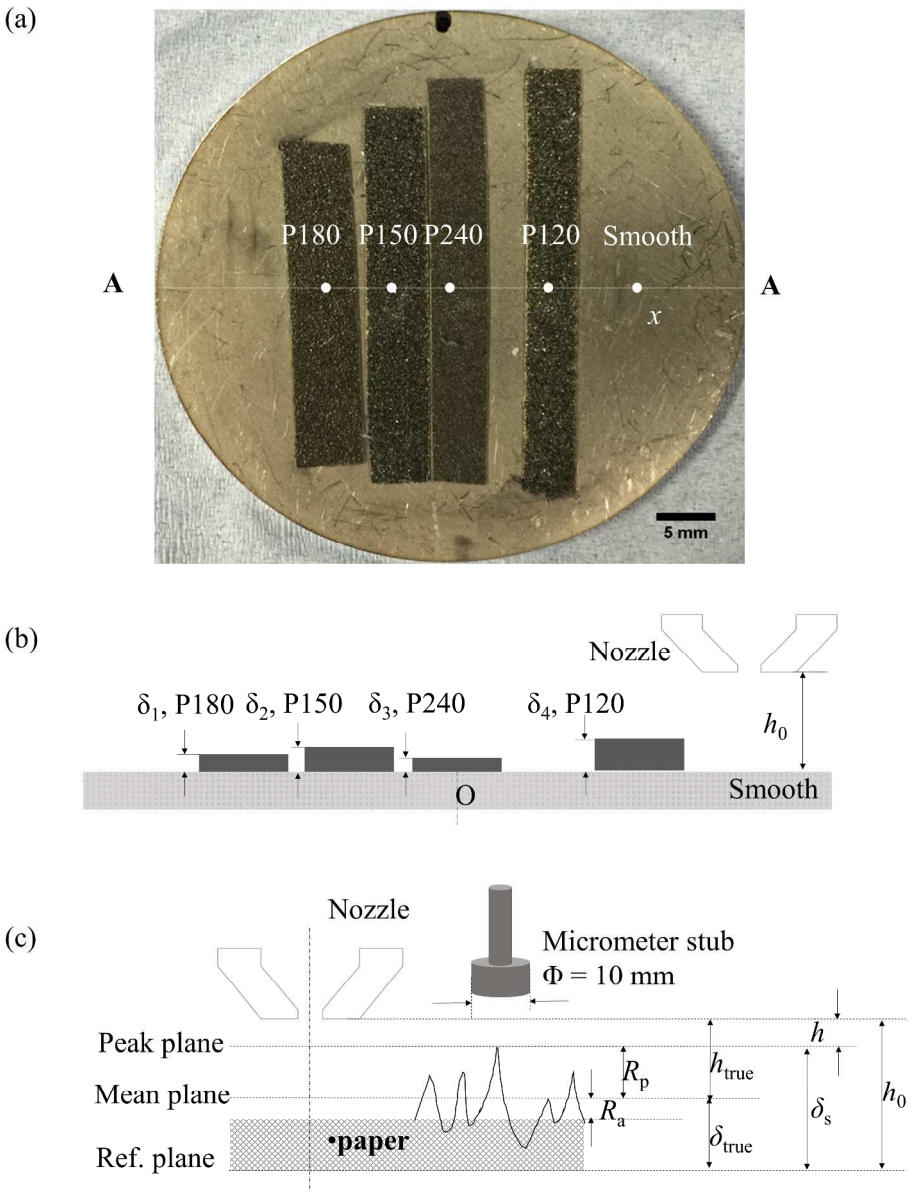

(a) Photograph, plan view of stainless steel disc with strips of sandpaper of different grit sizes attached. The gauging nozzle was moved across trajectory AA. Points indicate where gauging measurements were made; (b) Side view (not to scale) schematic of sandpaper thicknesses for zeroing, δ1-4 – thicknesses of sandpaper (P180, P150, P240 and P120, respectively); (c) Schematic (not to scale) of rough surface: Rp is the average height between highest peak and mean plane, Ra is the mean roughness, δs is the thickness measured by micrometer, δtrue the true thickness, htrue the corrected/true clearance from the nozzle to mean plane of sandpaper. The smooth substrate is the reference plane
1424x1833mm (72 x 72 DPI)

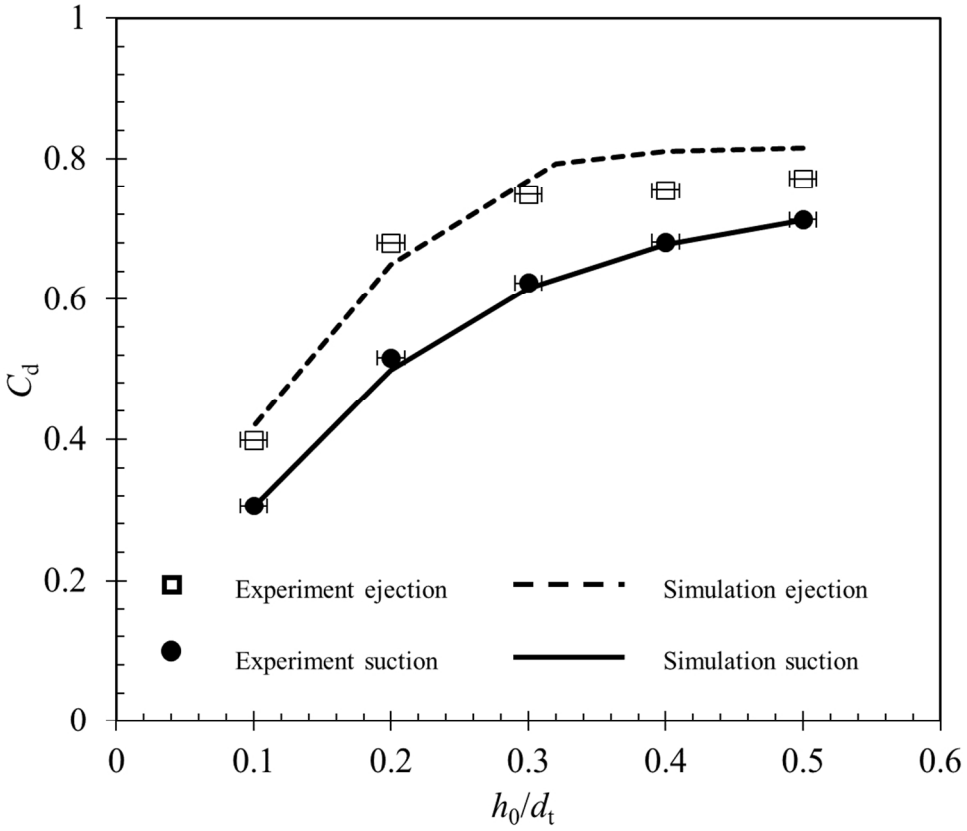

Reproducibility of ZFDG measurements on clean steel substrate. Deionised water at 16.5 °C, flow rate 20 ml/min. Ten data sets were collected at each h0/dt value from 0.1 to 0.5. The mean Cd value is plotted against h0/dt: the standard deviation is less than 0.2 % of each datum (not shown), and uncertainty in h is shown by horizontal error bars. Symbols: open – ejection, solid – suction; dashed line – CFD simulation of ejection test, solid line – simulation of suction tests
423x359mm (72 x 72 DPI)

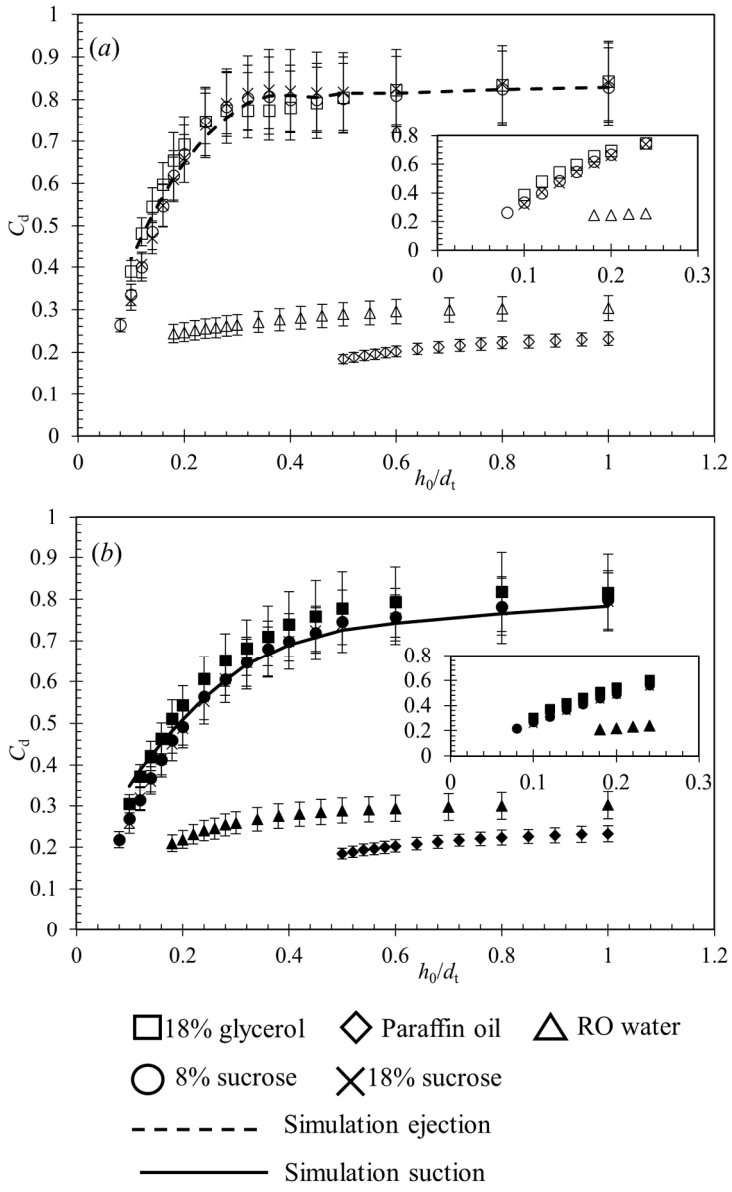

Calibration plots (Cd vs h0/dt) for the liquids in Table 1 at a flow rate of 20 ml/min, 16.5 °C. (a) ejection; (b) suction. Symbols: triangle – 18 wt% glycerol, Ret = 250; diamond – paraffin oil, Ret = 0.36; square – deionised water, Ret = 377; circle – 8 wt% sucrose solution, Ret = 349; cross – 10 wt% sucrose solution, Ret = 331. Dashed line – CFD simulation, ejection: solid line – CFD simulation, suction (both for deionised water). Inserts show Cd vs h0/dt in the usefully linear region
499x793mm (72 x 72 DPI)

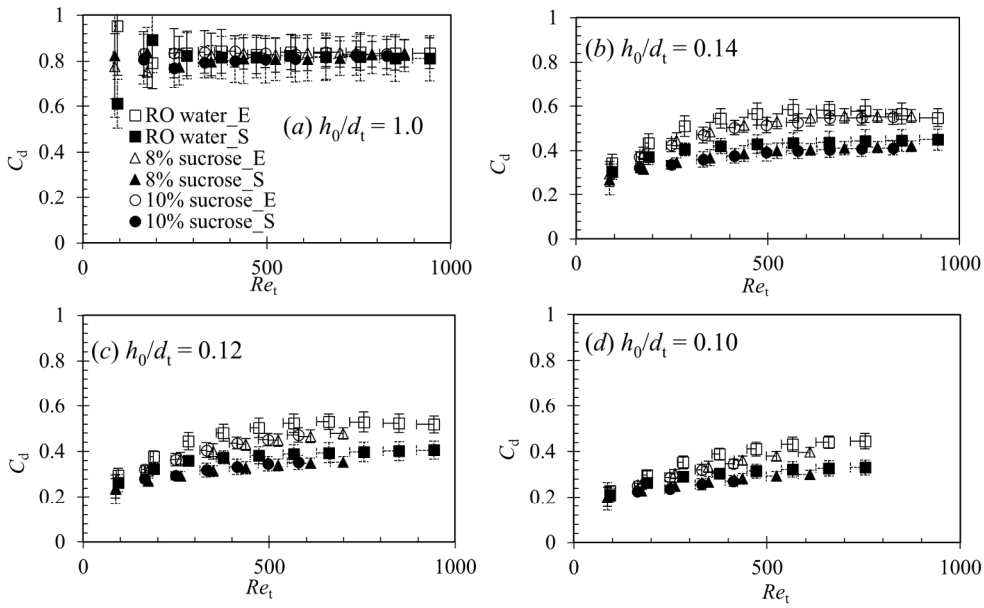

Effect of throat Reynolds number on Cd for deionised water (squares), 8 % sucrose solution (triangles) and 10 % sucrose solution (circles) in (i) ejection (open symbols) and (ii) suction (solid symbols) at (a) h0/dt = 1.0, (b) h0/dt = 0.14, (c) h0/dt = 0.12 and (d) h0/dt = 0.10
696x431mm (72 x 72 DPI)

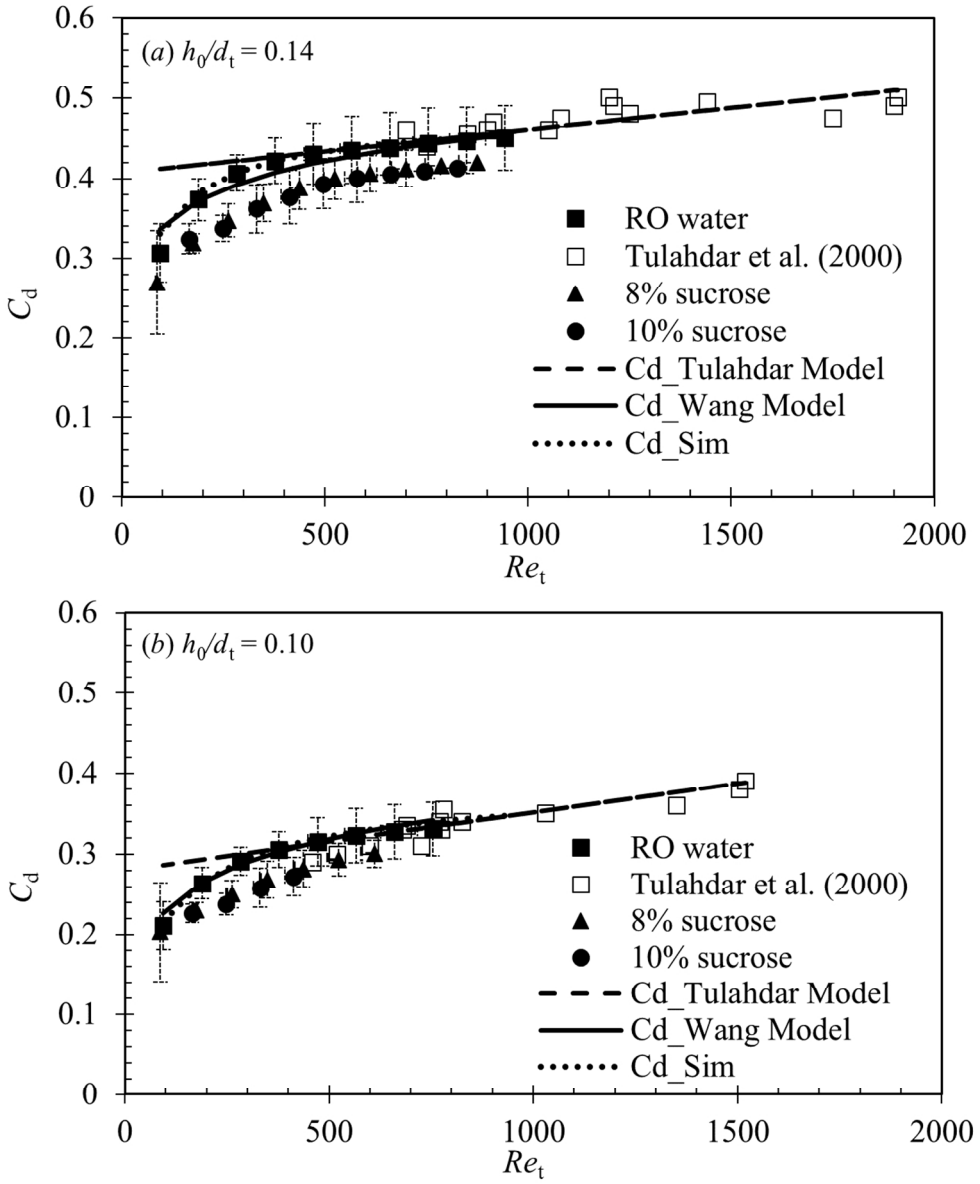

Comparison of experimental measurements, CFD simulations and Equations [6] and [10] for (a) h0/dt = 0.14 and (b) 0.10. Symbols, data: solid – this work, open – Tuladhar et al. [1]. Dashed line, Equation [6], solid lines, Equation [10], dotted lines – CFD simulation (deionized water). Gauging liquid: squares - deionised water, triangles - 8 % sucrose solution, circles - 10 % sucrose solution
459x552mm (72 x 72 DPI)

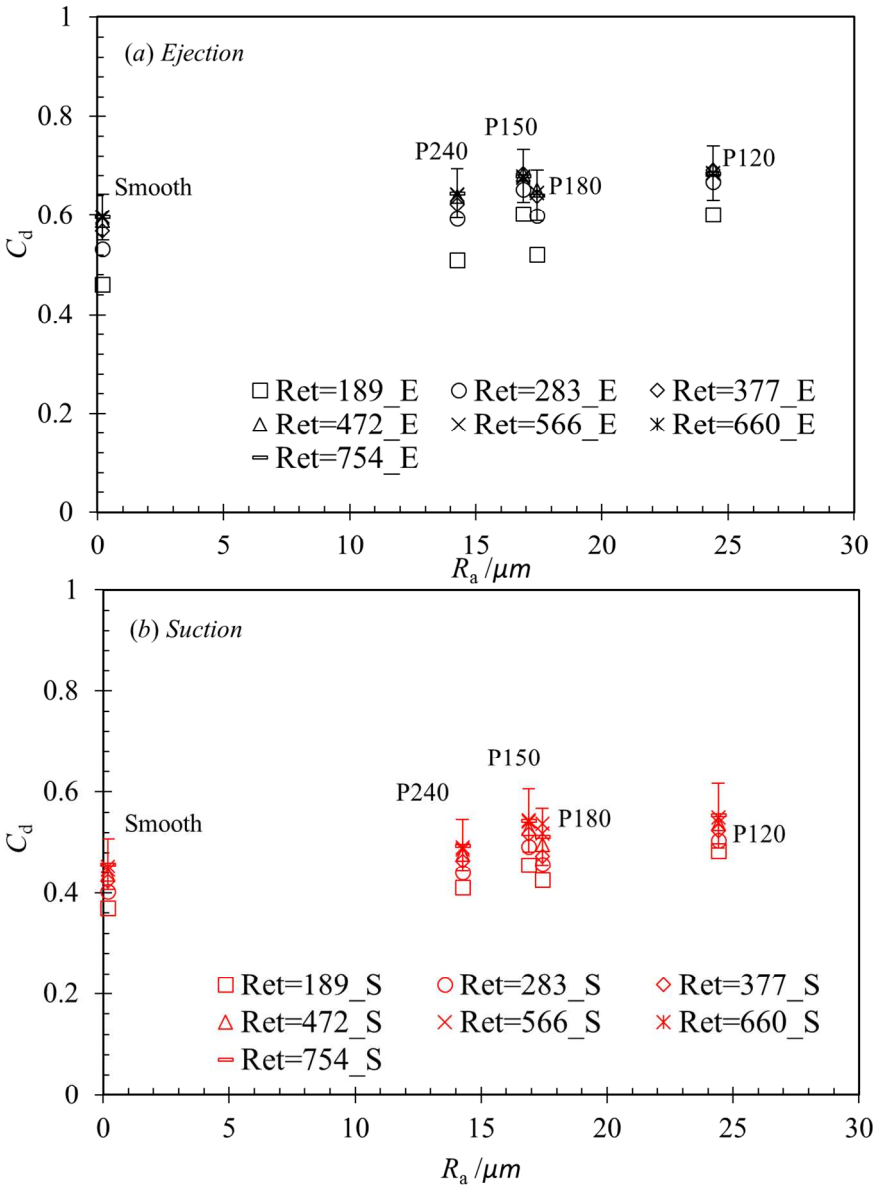

Effect of surface roughness, expressed as Ra, at Ret = 189 (square), 283 (circle), 377 (diamond), 472 (triangle), 566 (cross), 660 (asterisk) and 754 (dash) at initial nozzle-substrate clearance (not corrected for roughness) h/dt = 0.10. (a) ejection - black and (b) suction - red. The surfaces are (from left to right) smooth, P240, P150, P180 and P120 (note the roughness of P150 is lower than P180 due to the poor quality control (Mell [9]). Representative uncertainty bars shown for one dataset
461x615mm (72 x 72 DPI)

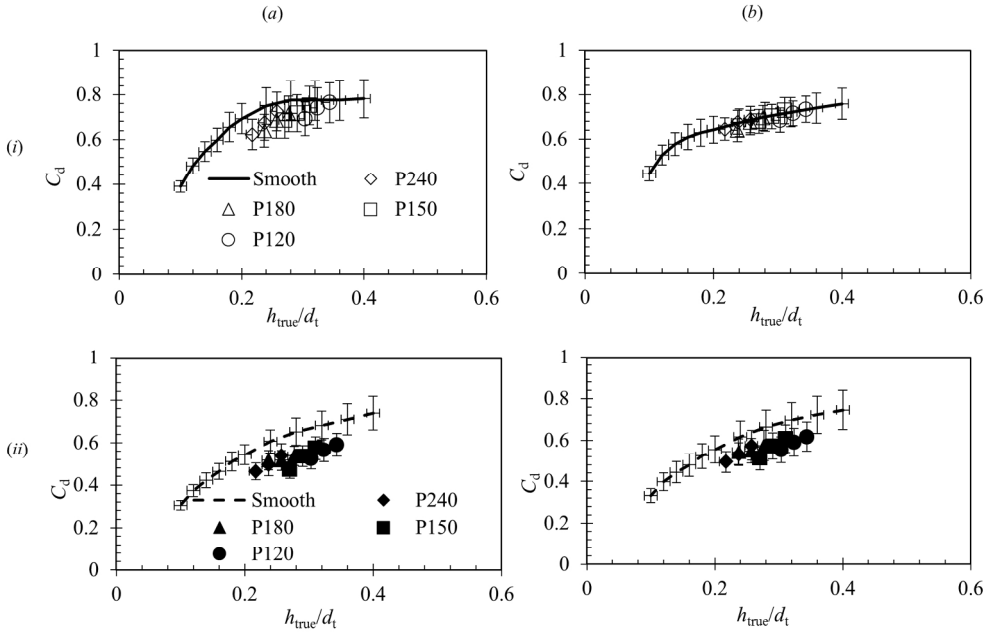

Calibration curves (Cd vs htrue/dt) on smooth and rough surfaces (the latter have been corrected for measured roughness). Symbols (Table 2): diamond – P240, triangle – P180, square – P150 and circle – P120. Gauging conditions: deionised water (16.5 °C), (a) Ret = 377 and (b) Ret = 754; (i) ejection, (ii) Suction. Loci are interpolations of experimental data for smooth surfaces
715x465mm (72 x 72 DPI)

Table 1. Physical properties of gauging liquids (16.5 ºC)

Gauging liquid	ρ	μ	Re_t (20 ml/min)	Supplier	Symbol
	kg/m^3	mPa.s	-		Figure 8
Deionised water	997.3	1.12	377	N/A	■/ □
8 wt% sucrose	1029.9	1.25	349	Sigma	▲
10 wt% surcrose	1038.1	1.33	331	Sigma	●
18 wt% glycerol	1047.6	1.65	250	Aldrich	N/A
Paraffin oil	860	1000	0.36	Sigma-Aldrich	N/A

Table 2. Sandpaper surface roughness measures, see Figure 4(b): R_a (arithmetical mean height), R_z (average height between highest peak and deepest valley), R_p (average height between highest peak and mean plane), and average particle sizes

Surface	R_a µm	R_z µm	R_p mm	Average particle diameter µm	Symbol Figure 10
Smooth	0.2	0.97	0.0007	N/A	Lines
P240*	~14.26	~169.6	0.12	68	◇
P180	17.43	198.1	0.14	82	△
P150	16.89	229.9	0.17	92 - 100	□
P120	24.41	273.2	0.20	115 - 125	○

* the data are for P220 due to lack of data on P240